Supporting Information

Ultrasmall MnO Nanoparticles Supported on Nitrogen-Doped Carbon Nanotubes as Efficient Anode Materials for Sodium Ion Batteries

Yanzhen He[†], Ping Xu *[†], Bin Zhang [†], Yunchen Du [†], Bo Song[‡], Xijiang Han *[†] and Huisheng Peng*[§]

[†]*MIIT Key Laboratory of Critical Materials Technology for New Energy Conversion and Storage, School of Chemistry and Chemical Engineering, Harbin Institute of Technology, Harbin 150001, China.*
[‡]*Academy of Fundamental and Interdisciplinary Sciences, Department of Physics, Harbin Institute of Technology, Harbin 150001, China.*
[§]*State Key Laboratory of Molecular Engineering of Polymers, Department of Macromolecular Science and Laboratory of Advanced Materials, Fudan University, Shanghai 200438, China.*

[*]Corresponding authors: pxu@hit.edu.cn (P.X.); hanxijiang@hit.edu.cn (X.H.); penghs@fudan.edu.cn (H.P.)

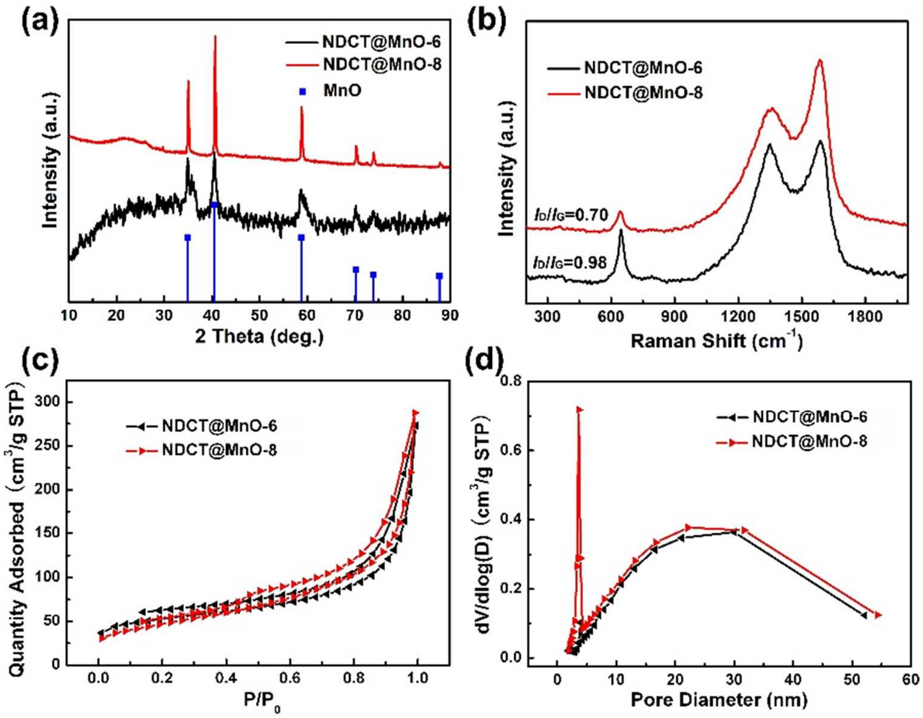

Figure S1. XRD patterns (a), Raman spectra (b), N_2 adsorption-desorption isotherms (c), and pore size distribution curves (d) of NDCT@MnO-6 and NDCT@MnO-8.

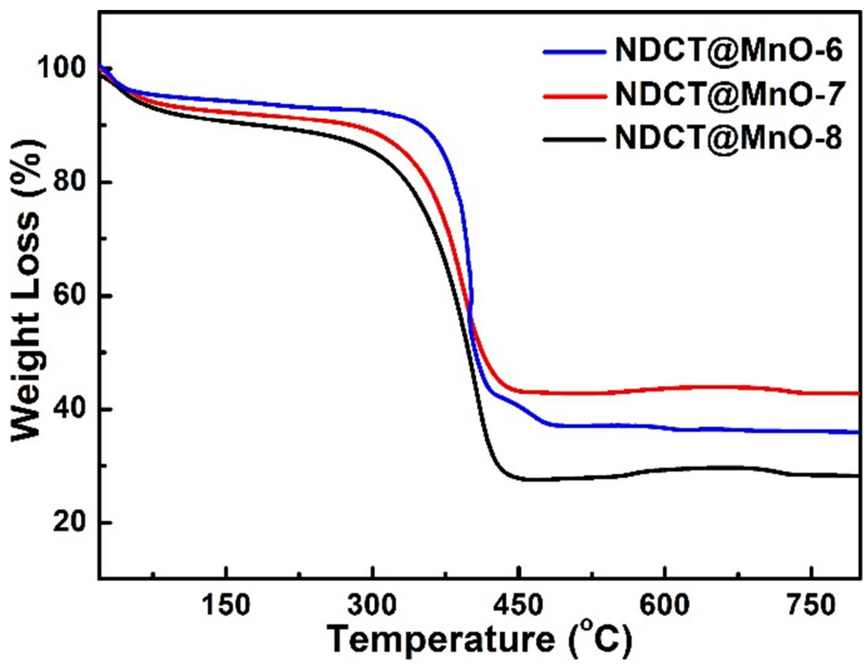

Figure S2. TGA curve of NDCT@MnO nanocomposite in air.

For NDCT@MnO-7 nanocomposites, a weight loss of 6.4% from room temperature to 150 °C is due to the removal of absorbed water. Subsequently, the weight loss from 150 to 800 °C can be attributed to both the combustion of carbon in air and oxidation of MnO to Mn_2O_3. The final remaining product (46.8%) will be only Mn_2O_3. The theoretical value of the weight increase from MnO to Mn_2O_3 is 11.27%. Thus, the actual amount of MnO in NDCT@MnO-7 nanocomposites can be calculated from: 46.8%/ (1+11.27%)=42.06%. Similarly, the amount of MnO in NDCT@MnO-6 and NDCT@MnO-8 was calculated to be 33.99% and 25.58%, respectively.

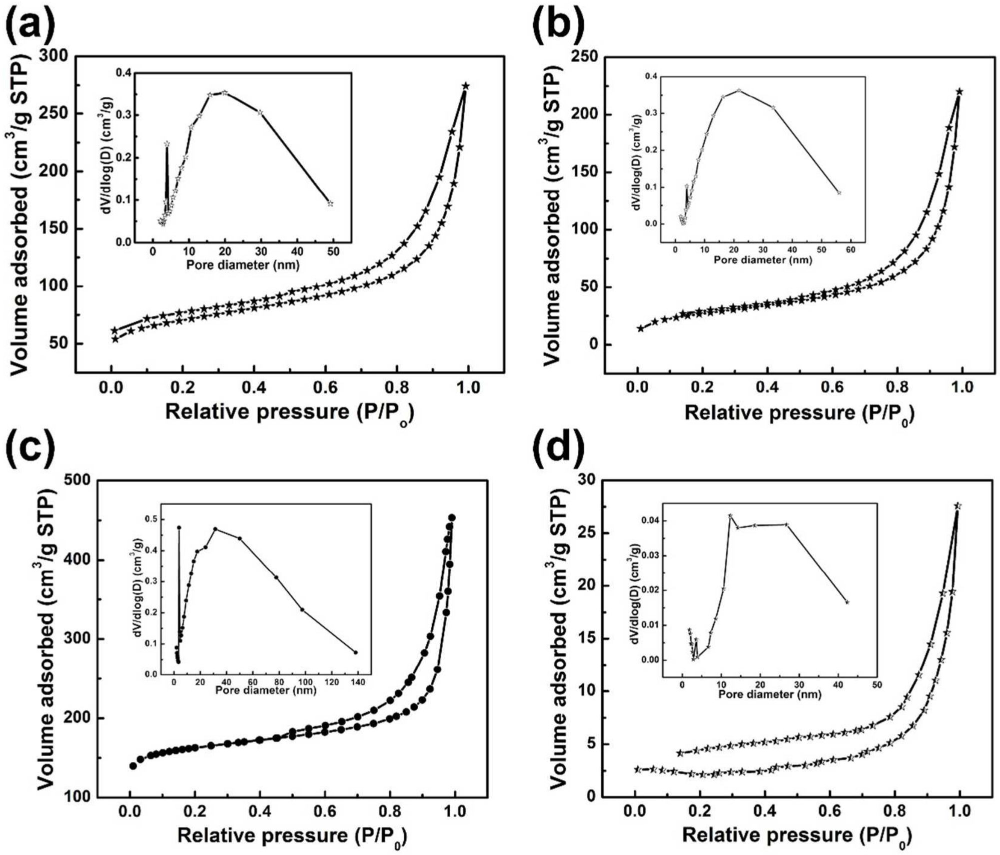

Figure S3. N_2 adsorption-desorption isotherms and pore size distribution (inset) of (a) NDCT@MnO-7, (b) PANI@Mn_3O_4, (c) NDCT, and (d) pure MnO.

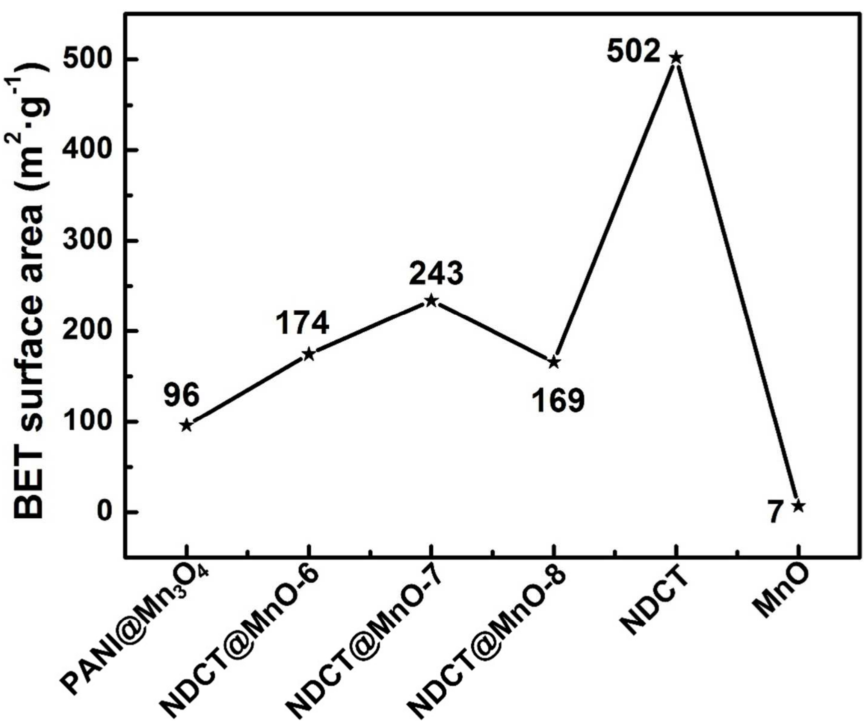

Figure S4. BET surface area of all as-prepared materials.

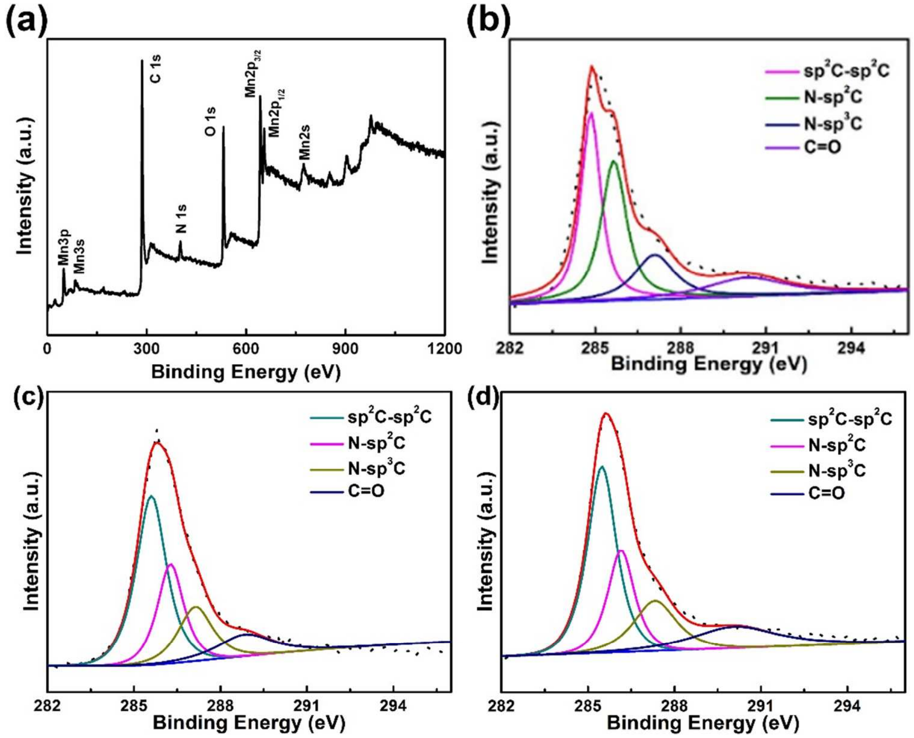

Figure S5. (a) Survey XPS spectrum of NDCT@MnO-7 nanocomposites, High-resolution C 1s XPS spectra of NDCT@MnO-7 (b), NDCT@MnO-6 (c), and NDCT@MnO-8 (d) nanocomposites.

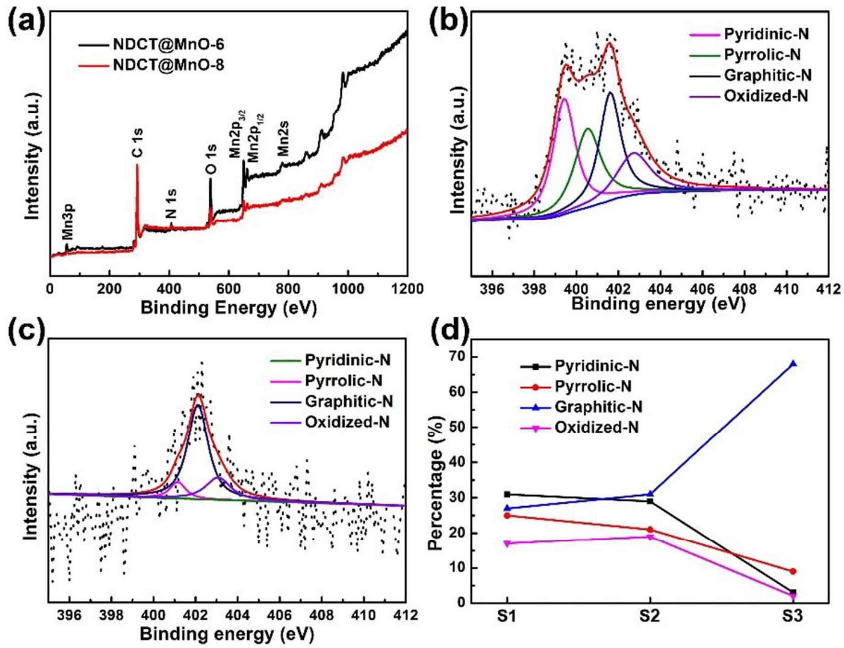

Figure S6. (a) Survey XPS spectrum of NDCT@MnO-6 and NDCT@MnO-8, High-resolution N 1s XPS spectra of NDCT@MnO-6 (b) and NDCT@MnO-8 (c), (d) Evolution of the content of different N species of NDCT@MnO nanocomposites as a function of the pyrolysis temperature. S1 is NDCT@MnO-6, S2 is NDCT@MnO-7, S3 is NDCT@MnO-8.

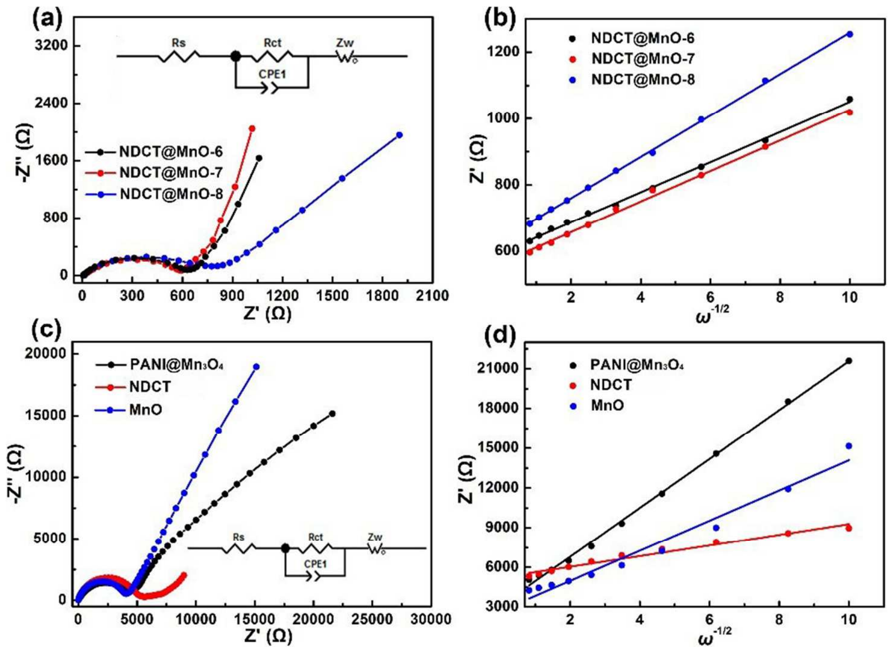

Figure S7 Nyquist dots of the NDCT@MnO (a), PANI@Mn_3O_4, NDCT-700, and MnO (c). Real parts of the impedance (Z') versus the reciprocal square root of angular frequency (ω) in the low frequency region of the NDCT@MnO samples (b), PANI@Mn_3O_4, NDCT-700, and MnO samples (d).

Figure S7a,c present the electrochemical impedance spectra (EIS) of the NDCT@MnO, PANI@Mn_3O_4, NDCT, and MnO materials. All the Nyquist plots are composed of a depressed semicircle from high to medium frequency followed by a slope line in the low frequency region, where the former is related to the charge transfer impedance (R_{ct}) at the electrode/electrolyte interfaces, and the latter corresponds to the Warburg impedance (Z_w) associated with Na^+ diffusion in the NDCT@MnO. R_s refers to the solution impedance, and constant-phase element (CPE) represents the double-layer capacitance, taking into account the roughness of the particle surface.

EIS is an important tool to evaluate the diffusion coefficient of Na^+ ions (D_{Na}) within the electrode:

$$D_{Na} = \frac{R^2T^2}{2A^2n^4F^4C^2\sigma^2} \qquad \text{(S1)}$$

In Eq. S1, R is the gas constant, T is the absolute temperature, A is the surface area of electrode, n is the number of electrons per molecule during oxidization, F is the Faraday constant, C is the concentration of sodium ion, and σ is the Warburg factor, σ relates to Z' through Eq. S2 and its value can be obtained from the slope of the line between Z' and $\omega^{1/2}$ as shown in Figure S7b,d.

$$Z' = R_s + R_{ct} + \sigma\omega^{-1/2} \qquad \text{(S2)}$$

As can be calculated, the σ value of NDCT@MnO-7 is the smallest, reflecting the largest D_{Na} (Table S3). This further demonstrates that the N-doping and the uniformly dispersed ultrasmall MnO nanoparticles can facilitate the Na^+ ions diffusion kinetics.

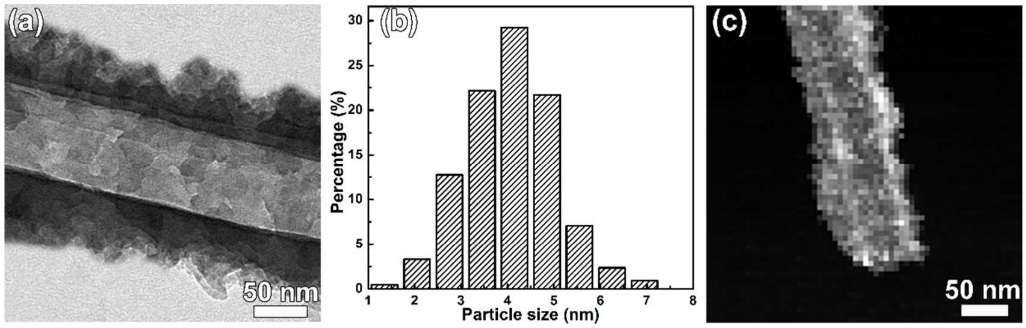

Figure S8. (a) TEM image of PANI nanotubes. (b) Particle size distribution diagram of MnO nanoparticles in NDCT@MnO-7. (c) STEM image of NDCT@MnO-7 nanocomposites.

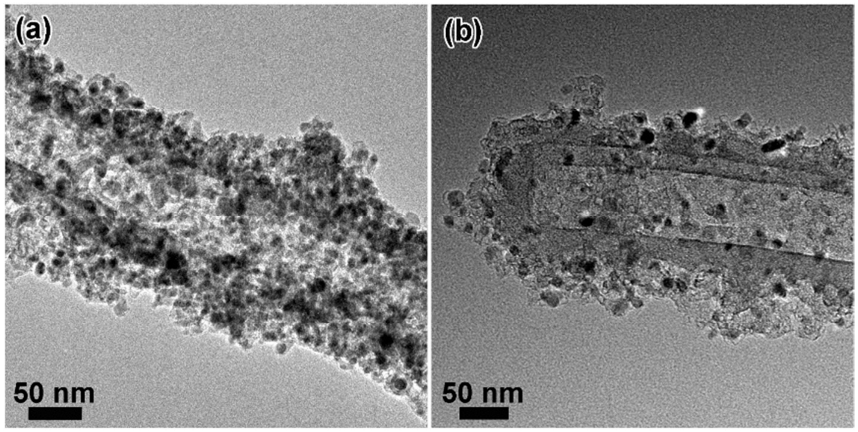

Figure S9. TEM images of NDCT@MnO-6 (a) and NDCT@MnO-8 (b).

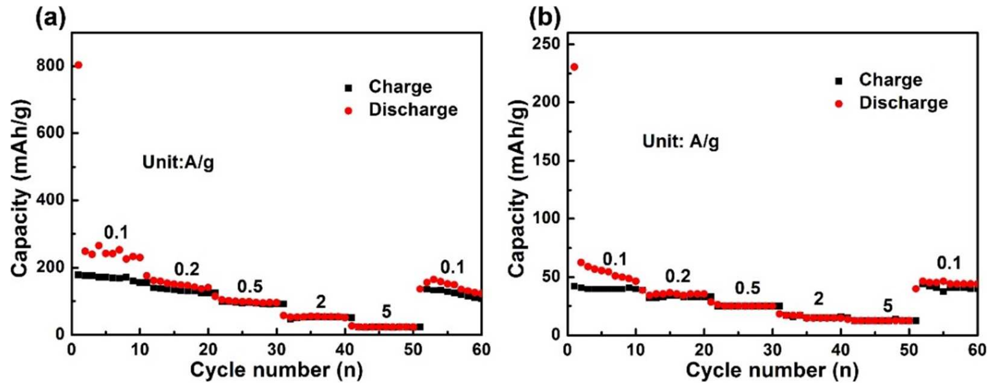

Figure S10. Rate capability of (a) NDCT and (b) free MnO in the potential window of 0.01~3.0 V *vs.* Na/Na^{+}.

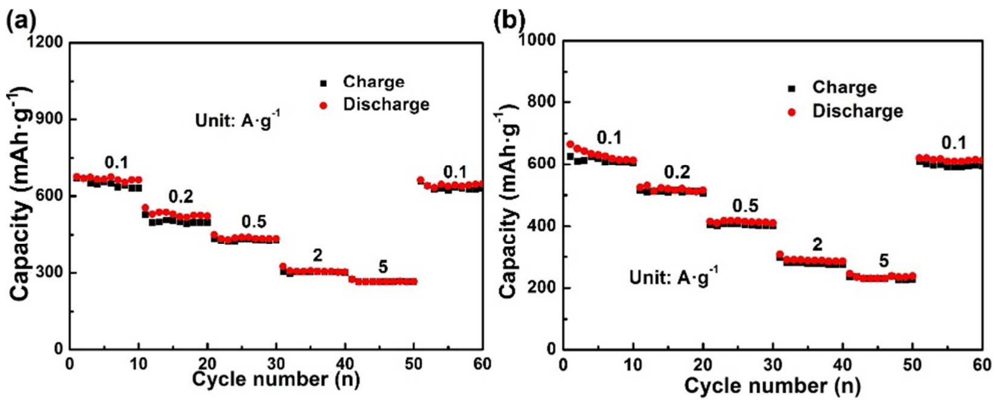

Figure S11. Rate capability of NDCT@MnO-6 (a) and NDCT@MnO-8 (b) in the potential window of 0.01~3.0 V *vs*. Na/Na^+.

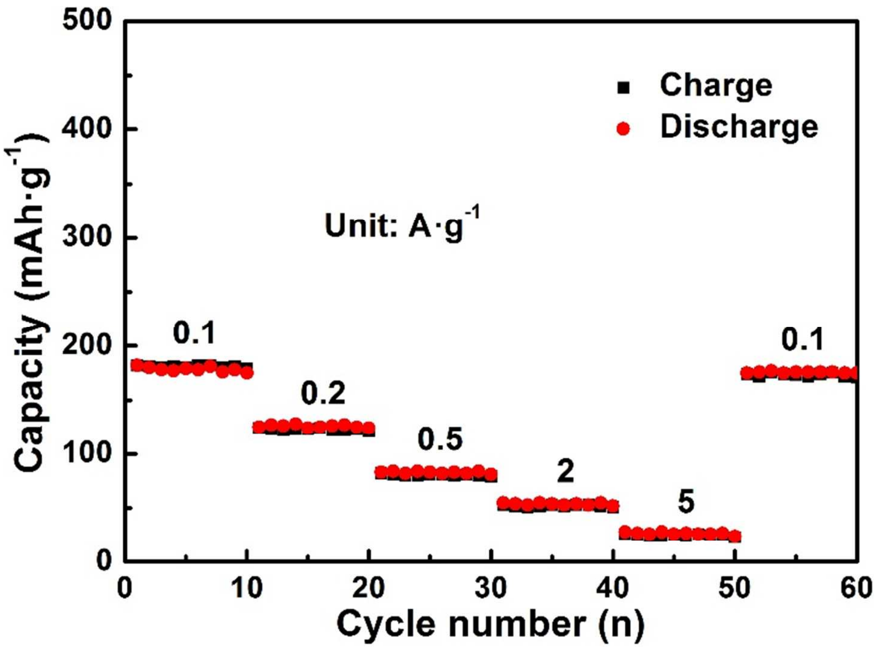

Figure S12. Rate capability of PANI@Mn_3O_4 in the potential window of 0.01~3.0 V *vs.* Na/Na^+.

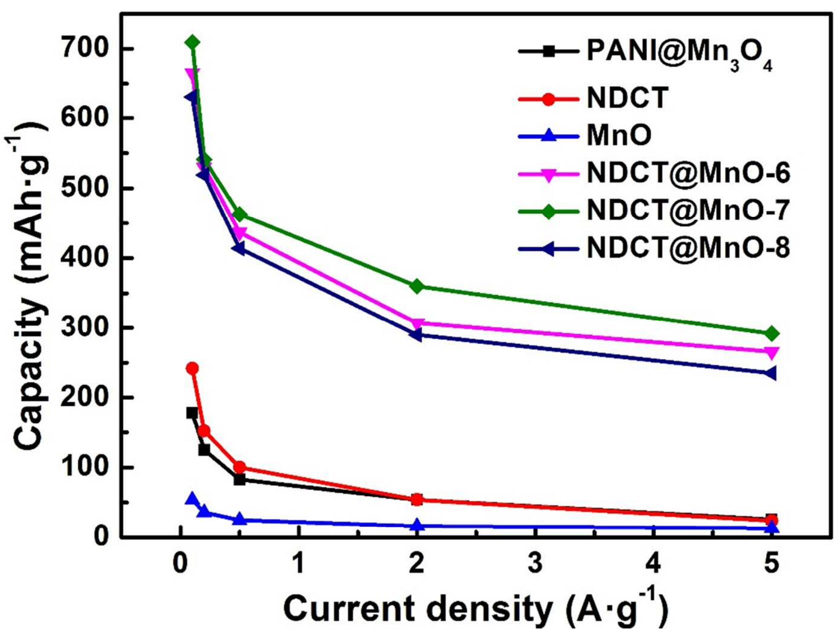

Figure S13. Rate capability of PANI@Mn_3O_4, NDCT, NDCT@MnO, and MnO.

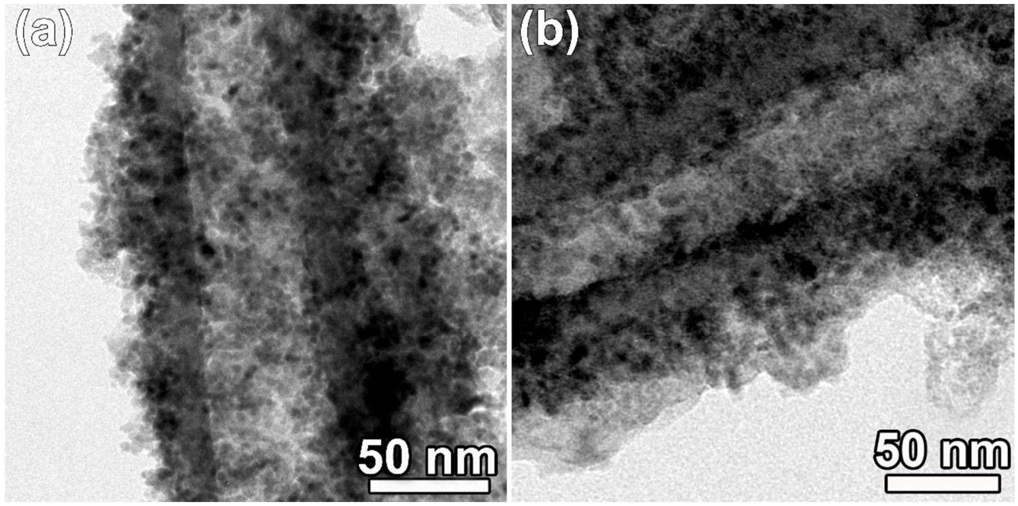

Figure S14. TEM images of NDCT@MnO-7 electrode. (a) sodiated (after the 1st discharge), (b) desodiated (after the 1st charge).

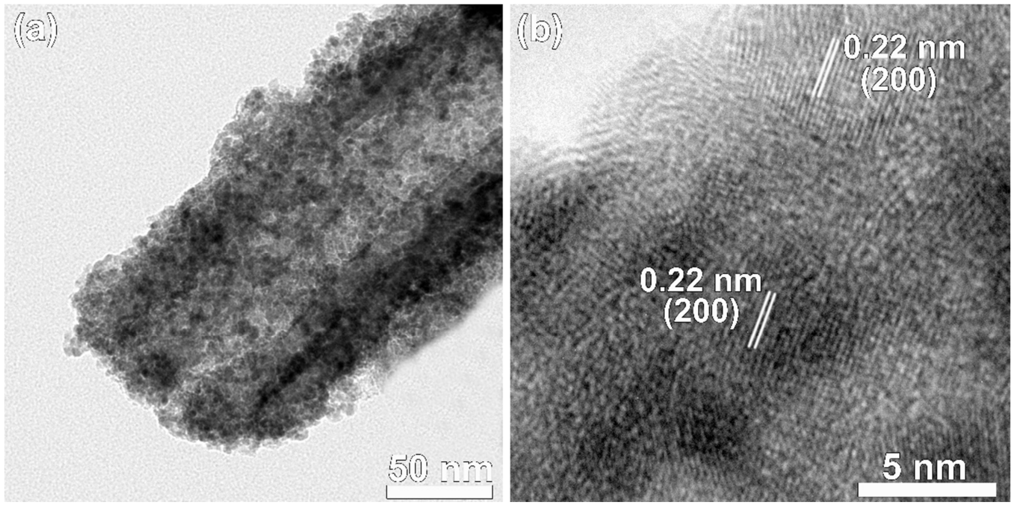

Figure S15. (a) TEM and (b) HRTEM images of NDCT@MnO-7 nanocomposites after 3000 cycles at 5 A g^{-1}.

Table S1 The content of various N species (atomic ratio, %)

Materials	Total content of N	Pyridinic-N	Pyrrolic-N	Graphitic-N	Oxidized-N
NDCT@MnO-6	5.43	31	25	27	17
NDCT@MnO-7	4.75	29	21	31	19
NDCT@MnO-8	1.62	3	9	68	2

Table S2 Electrical conductivity of the as-prepared materials from a four-probe method.

Materials	σ ($S \cdot m^{-1}$)
MnO	$<9.4\times10^{-6}$
NDCT-700	14.6
PANI@Mn_3O_4	$<9.4\times10^{-6}$
NDCT@MnO-6	0.25
NDCT@MnO-7	0.37
NDCT@MnO-8	0.20

Table S3 Simulated results corresponding to the ESI data shown in Figure S7.

Sample	R_s (Ω)	R_{ct} (Ω)	σ (Ω cm $s^{-1/2}$)	D_{Na} ($cm^2\ s^{-1}$)
NDCT@MnO-8	5.4	647.9	62.4	2.7×10^{-12}
NDCT@MnO-7	4.1	618	45.4	4.8×10^{-12}
NDCT@MnO-6	4.6	623.2	47.2	4.4×10^{-12}
PANI@Mn_3O_4	19.3	4071	1246.1	8.9×10^{-17}
NDCT-700	13.37	2690	404.8	2.1×10^{-15}
MnO	20.1	3980	1139.1	1.7×10^{-16}

Table S4. Specific capacities of NDCT, free MnO nanoparticles and NDCT@MnO nanocomposites at different current densities.

Current density (A g^{-1})	0.1	0.2	0.5	2	5
PANI@Mn_3O_4 (mAh g^{-1})	178	125	83	54	26
NDCT (mAh g^{-1})	242	152	100	54	24
NDCT@MnO-6 (mAh g^{-1})	665	530	437	307	266
NDCT@MnO-7 (mAh g^{-1})	709	541	463	360	292
NDCT@MnO-8 (mAh g^{-1})	631	519	414	290	235
Free MnO (mAh g^{-1})	54	36	25	16	13

Table S5. Comparison of electrochemical performance of transition metal oxides anodes for SIBs.

Materials	Current density (A g^{-1})	Cycle number	Capacity (mAh g^{-1})	Reference
NDCT@MnO	**5**	**3000**	**273**	**This work**
Co_3O_4/N-doped carbon	0.5	50	276	[1]
MnOOH	0.5	50	223.1	[2]
Nitrogen doped/carbon tuning yolk-like TiO_2	0.168	200	243.2	[3]
Carbon-coated TiO_2 nano-olives	0.336	1000	125	[4]
2 nm CuO quantum dots@carbon nanofibers	0.5	500	401	[5]
Fe_3O_4@carbon nanotube	0.1	300	377	[6]
$MnCoNiO_x$@double carbon	0.1	500	230	[7]
Fe_2O_3@graphene composite nanosheets	2	500	110	[8]
graphene-Fe_3O_4	0.05	200	312	[9]
Graphene@nitrogen doped carbon@TiO_2	1	5000	109	[10]
Multi-walled carbon nanotubes@Fe_2O_3@C	0.16	100	272	[11]
Co_3O_4@nitrogen-doped carbon	1	1100	175	[12]

References

(1) Kang, W.; Zhang, Y.; Fan, L.; Zhang, L.; Dai, F.; Wang, R.; Sun, D., Metal-Organic Framework Derived Porous Hollow Co_3O_4/N-C Polyhedron Composite with Excellent Energy Storage Capability. *ACS Appl. Mater. Interfaces* **2017,** *9*, 10602-10609.

(2) Shao, L.; Zhao, Q.; Chen, J., MnOOH Nanorods as High-Performance Anodes for Sodium Ion Batteries. *Chem. Commun.* **2017,** *53*, 2435-2438.

(3) Zhang, Y.; Wang, C.; Hou, H.; Zou, G.; Ji, X., Nitrogen Doped/Carbon Tuning Yolk-Like TiO_2 and Its Remarkable Impact on Sodium Storage Performances. *Adv. Energy Mater.* **2017,** *7*, 1600173.

(4) Chen, J.; Zhang, Y.; Zou, G.; Huang, Z.; Li, S.; Liao, H.; Wang, J.; Hou, H.; Ji, X., Size-Tunable Olive-Like Anatase TiO_2 Coated with Carbon as Superior Anode for Sodium-Ion Batteries. *Small* **2016,** *12*, 5554-5563.

(5) Wang, X.; Liu, Y.; Wang, Y.; Jiao, L., CuO Quantum Dots Embedded in Carbon Nanofibers as Binder-Free Anode for Sodium Ion Batteries with Enhanced Properties. *Small* **2016,** *12*, 4865-4872.

(6) Wang, X.; Liu, X.; Wang, G.; Xia, Y.; Wang, H., One-Dimensional Hybrid Nanocomposite of High-Density Monodispersed Fe_3O_4 Nanoparticles and Carbon Nanotubes for High-Capacity Storage of Lithium and Sodium. *J. Mater. Chem. A* **2016,** *4*, 18532-18542.

(7) Wu, L.; Lang, J.; Wang, R.; Guo, R.; Yan, X., Electrospinning Synthesis of Mesoporous $MnCoNiO_x$@Double-Carbon Nanofibers for Sodium-Ion Battery Anodes with Pseudocapacitive Behavior and Long Cycle Life. *ACS Appl. Mater. Interfaces* **2016,** *8*, 34342-34352.

(8) Li, D.; Zhou, J.; Chen, X.; Song, H., Amorphous Fe_2O_3/Graphene Composite Nanosheets with Enhanced Electrochemical Performance for Sodium-Ion Battery. *ACS Appl. Mater. Interfaces* **2016,** *8*, 30899-30907.

(9) Liu, H.; Jia, M.; Zhu, Q.; Cao, B.; Chen, R.; Wang, Y.; Wu, F.; Xu, B., 3D-0D Graphene-Fe_3O_4 Quantum Dot Hybrids as High-Performance Anode Materials for Sodium-Ion Batteries. *ACS Appl. Mater. Interfaces* **2016,** *8*, 26878-26885.

(10) Zhang, Z.; An, Y.; Xu, X.; Dong, C.; Feng, J.; Ci, L.; Xiong, S., Metal-Organic Framework-Derived Graphene@Nitrogen Doped Carbon@Ultrafine TiO_2 Nanocomposites as High Rate and Long-Life Anodes for Sodium Ion Batteries. *Chem. Commun.* **2016,** *52*, 12810-12812.

(11) Zhao, Y.; Feng, Z.; Xu, Z. J., Yolk-Shell Fe_2O_3 Middle Dot in Circle C Composites Anchored on MWNTs with Enhanced Lithium and Sodium Storage. *Nanoscale* **2015,** *7*,

9520-9525.

(12) Wang, Y.; Wang, C.; Wang, Y.; Liu, H.; Huang, Z., Superior Sodium-Ion Storage Performance of Co_3O_4@Nitrogen-Doped Carbon: Derived from a Metal-Organic Framework. *J. Mater. Chem. A* **2016,** *4*, 5428-5435.